Jeremie Boucher,[1] Samir Softic,[1,2] Abdelfattah El Ouaamari,[3] Megan T. Krumpoch,[1] Andre Kleinridders,[1] Rohit N. Kulkarni,[3] Brian T. O'Neill,[1] and C. Ronald Kahn[1]

Differential Roles of Insulin and IGF-1 Receptors in Adipose Tissue Development and Function

Diabetes 2016;65:2201–2213 | DOI: 10.2337/db16-0212

To determine the roles of insulin and insulin-like growth factor 1 (IGF-1) action in adipose tissue, we created mice lacking the insulin receptor (IR), IGF-1 receptor (IGF1R), or both using Cre-recombinase driven by the adiponectin promoter. Mice lacking IGF1R only (F-IGFRKO) had a ~25% reduction in white adipose tissue (WAT) and brown adipose tissue (BAT), whereas mice lacking both IR and IGF1R (F-IR/IGFRKO) showed an almost complete absence of WAT and BAT. Interestingly, mice lacking only the IR (F-IRKO) had a 95% reduction in WAT, but a paradoxical 50% increase in BAT with accumulation of large unilocular lipid droplets. Both F-IRKO and F-IR/IGFRKO mice were unable to maintain body temperature in the cold and developed severe diabetes, ectopic lipid accumulation in liver and muscle, and pancreatic islet hyperplasia. Leptin treatment normalized blood glucose levels in both groups. Glucose levels also improved spontaneously by 1 year of age, despite sustained lipodystrophy and insulin resistance. Thus, loss of IR is sufficient to disrupt white fat formation, but not brown fat formation and/or maintenance, although it is required for normal BAT function and temperature homeostasis. IGF1R has only a modest contribution to both WAT and BAT formation and function.

Insulin and insulin-like growth factor 1 (IGF-1) play important roles in the development and differentiation of white and brown adipose tissue (WAT and BAT) (1,2). These hormones act through insulin and IGF-1 receptors (IR and IGF1R), which are highly homologous and share many overlapping downstream signaling pathways. Furthermore, whereas insulin and IGF-1 bind with higher affinity to their cognate receptors, insulin can also bind and activate the IGF1R and vice versa (3,4). In preadipocytes, IGF1R expression is higher than IR expression, whereas in mature adipocytes the opposite is true (3,5). Fat-specific deletion of IR results in reduced WAT and BAT mass (6,7), whereas mice with a fat-specific deletion of IGF1R alone have been reported to have slightly increased adipose tissue mass associated with increased overall body growth (8). Deletion of both receptors in fat leads to a marked reduction in WAT and BAT mass and obesity resistance, even when challenged with a high-fat diet (9).

One limitation of many of these previous studies is that conditional inactivation of the receptors was achieved using a targeting approach based on the expression of the Cre-recombinase under the control of aP2 promoter. This can lead to a variable degree of recombination efficiency in different fat depots, as well as potentially important off-target recombination events (10–13). In the current study, we deleted the IR and/or IGF1R specifically in adipose tissues using the adiponectin-Cre (Adipo-Cre) transgene, which produces more uniform and efficient deletion and is completely adipocyte specific (10–13). In this study, we show that in WAT, the IGF1R plays only a modest role,

[1]Section on Integrative Physiology and Metabolism, Joslin Diabetes Center and Department of Medicine, Harvard Medical School, Boston, MA
[2]Division of Gastroenterology, Hepatology and Nutrition, Boston Children's Hospital, Boston, MA
[3]Islet Cell and Regenerative Medicine, Joslin Diabetes Center and Department of Medicine, Harvard Medical School, Boston, MA

Corresponding author: C. Ronald Kahn, c.ronald.kahn@joslin.harvard.edu.

Received 11 February 2016 and accepted 6 May 2016.

This article contains Supplementary Data online at http://diabetes.diabetesjournals.org/lookup/suppl/doi:10.2337/db16-0212/-/DC1.

J.B. and S.S. contributed equally to this work.

J.B. is currently affiliated with Cardiovascular and Metabolic Diseases iMed, AstraZeneca R&D, Mölndal, Sweden.

A.K. is currently affiliated with German Institute of Human Nutrition, Potsdam-Rehbruecke, Germany, and German Center for Diabetes Research (DZD), Neuherberg, Germany.

See accompanying article, p. 2187.

whereas mice lacking IR alone or both IR and IGF1R display a lipodystrophic phenotype with severe diabetes, insulin resistance, and ectopic fat distribution in both muscle and liver. BAT mass, in contrast, is differentially regulated and only decreased when both IR and IGF1R are absent, thus indicating a more integrated role of these receptors in BAT.

RESEARCH DESIGN AND METHODS

Animals and Diets

All protocols were approved by the Institutional Animal Care and Use Committee of the Joslin Diabetes Center and were in accordance with National Institutes of Health guidelines. Mice were housed at 20–22°C on a 12-h light/dark cycle with ad libitum access to water and food (Mouse Diet 9F; PharmaServ). Fat-specific IR, IGF1R, and IR/IGF1R knockout (F-IRKO, F-IGFRKO, and F-IR/IGFRKO, respectively) mice were generated by breeding $IR^{lox/lox}$/$IGF1R^{lox/lox}$ mice on a C57BL/6-129Sv genetic background (9) with mice carrying Cre recombinase driven by the adiponectin promoter (Adipo-Cre) on a C57BL/6 background (12). $IR^{lox/+}$/$IGF1R^{lox/+}$ heterozygous mice were bred to generate Adipo-Cre homozygous littermate mice for all three genotypes. Adipo-Cre–positive males and Adipo-Cre–negative female mice of each genotype were used for breeding, and breeder pairs of each genotype were replaced simultaneously every 6 months to ensure that there is little or no genetic drift. Male mice were used throughout the study, and control (Adipo-Cre negative floxed) mice from all three genotypes were pooled into a single control group, because none demonstrated physiological abnormalities.

Insulin Tolerance Test and Leptin Treatment

Insulin tolerance tests were performed after a 2-h fast with 1.25 units of insulin/kg for control and F-IGFRKO mice and 2 units/kg for F-IRKO and F-IR/IGFRKO mice (Humulin R; Lilly). Glucose levels were measured using a glucose meter (Infinity; US Diagnostics). Leptin (10 μg/mouse/day; Sigma-Aldrich) or saline was administered using osmotic pumps (Alzet Model 1002; Alzet) inserted subcutaneously in 3-month-old mice for 14 days.

Serum Analyses

Serum parameters were determined by the Joslin Diabetes and Endocrinology Research Center assay core using commercial kits. Hormones were assessed by ELISA, adipokines were measured by a multiplex assay, and triglycerides (TG), cholesterol, and free fatty acids (FFA) were assessed by colorimetric assays.

Body Temperature and Cold Exposure

Body temperature was measured in 3-month-old mice using a RET-3 rectal probe (Physitemp). For cold exposure, mice were housed individually at an ambient temperature of 6°C. Temperature was measured every 30 min for 3 h or until body temperature dropped below 25°C.

Measurement of β-Cell Proliferation and Islet Area

Pancreatic tissue was immunostained using anti-Ki67 (BD Biosciences) and anti-insulin (Abcam) antibodies. $Ki67^+$ β-cells were visualized by immunofluorescence microscopy and counted by a blinded observer (14). Insulin-positive cells colocalized with nuclear DAPI and Ki67 immunostaining were counted as proliferating β-cells. β-Cell area was determined by ImageJ software (National Institutes of Health) and calculated as insulin-positive area divided by total pancreas area.

Gene Expression Analysis

mRNA extraction and quantification was performed as previously described (9).

Protein Extraction and Immunoblot Analysis

Muscle tissue was frozen, pulverized, and homogenized in radioimmunoprecipitation assay buffer (Millipore) with protease and phosphatase 2 and 3 inhibitors (Sigma-Aldrich). Lysates were subjected to SDS-PAGE, transferred to polyvinylidene difluoride membranes (Thermo Scientific), and blotted using IRβ (Santa Cruz Biotechnology), Glut4 (Chemicon International), or β-actin–horseradish peroxidase (Santa Cruz Biotechnology) antibodies. Quantification of immunoblots was performed using ImageJ (National Institutes of Health).

Histology and Muscle Fiber Size

Frozen cross-sections of tibialis anterior (TA) muscle were fixed in 4% paraformaldehyde for 5 min, washed, permeabilized with 0.5% Triton X-100, and immunofluorescently stained for laminin (L9393; 1:200 dilution; Sigma-Aldrich) with Alexa Fluor 488–conjugated secondary antibodies (1:500; Life Technologies). Images of laminin-stained fibers were taken in the same superficial area of TA muscles and then changed to grayscale using Adobe Photoshop (v6.0; Adobe Systems). ImageJ software (National Institutes of Health) was used to threshold images, and the "Analyze Particles" tool was used to find all cross-sections between 500 and 1,000,000 square pixels with circularity of 0.5–1.0. Pixel area was converted to micrometers squared by quantifying the length of the 200-μm scale bar in pixels.

Muscle Lipid Accumulation, Succinate Dehydrogenase, and Nile Red Costaining

Cross-sections of TA muscle were stained for succinate dehydrogenase (SDH) as previously described (15). After SDH staining, sections were rinsed in ice-cold PBS, fixed in 4% paraformaldehyde, and washed with PBS. Sections were then incubated in a 1:10,000 dilution of 1 mg/mL Nile Red (N-1142; ThermoFisher Scientific), washed twice with PBS, and mounted with SlowFade Gold with DAPI (S36938; Life Technologies). Skeletal muscle and heart TG were quantified as previously described (16).

Mitochondrial Nuclear to DNA Ratio and Oxygen Consumption

Mitochondrial DNA content was assessed by quantitative PCR (Applied Biosystems 7900; Applied Biosystems) using primers for five different mitochondrial-encoded genes (ND1, ND4, cyclooxygenase 2 and 3, and rRNA) and two different nuclear-encoded genes (Chdh and Actb). Results are expressed as an average of the different mitochondrial to nuclear DNA ratios.

BAT oxygen consumption rate was assessed using freshly isolated mouse BAT as previously described (17). Briefly, BAT was rinsed with unbuffered Krebs-Henseleit buffer media, cut into pieces (~10 mg), and washed extensively. Each piece was placed in a single well of a XF24-well Islet Flux plate (#101174-100; Seahorse Bioscience, North Billerica, MA) and analyzed in a Seahorse XF24 Analyzer. Each optical character recognition value was an average of five independent pieces per tissue per experiment and adjusted to total DNA content.

Statistical Analyses

All data are presented as mean ± SEM and analyzed by unpaired two-tailed Student *t* test or ANOVA as appropriate.

RESULTS

Generalized Lipodystrophy in Mice Lacking IR in the Fat

Mice with a homozygous fat-specific knockout of the IR, IGF1R, or both were generated by breeding mice with IR and IGF1R floxed alleles (9) and mice carrying a Cre-recombinase transgene driven by the adiponectin promoter (12). By 3 months of age, male F-IGFRKO mice displayed a ~25% decrease in subcutaneous (inguinal) and visceral (epididymal) WAT weight, whereas F-IRKO mice displayed a >90% reduction in weights of both WAT depots (Fig. 1*A*). Visceral WAT in F-IRKO mice displayed dramatically reduced cell size, whereas the residual subcutaneous WAT was a mixture of connective tissue, undifferentiated cells, and a few lipid-laden adipocytes (Fig. 1*B*). The fibroblast-like cells could be preadipocytes or dedifferentiated adipocytes, or even dying differentiated adipocytes, or just be a residue of the stromavascular fraction of a normal adipose tissue depot. Mice with knockout of both IR and IGF1R had no apparent visceral WAT and a 99% reduction in subcutaneous WAT with few identifiable adipocytes (Fig. 1*A* and *B*).

Consistent with the reduction in fat mass, circulating leptin, resistin, and adiponectin levels were markedly decreased in F-IRKO and F-IR/IGFRKO mice (Fig. 1*C*). Despite its normal appearance, F-IGFRKO WAT displayed 30–50% decreases in *Glut4*, *Fas*, *Hsl*, *leptin*, and *adiponectin* mRNA (Fig. 1*D*). These genes were more robustly decreased in F-IRKO WAT, which also exhibited reduced mRNA levels of *Atgl* (50%), *resistin* (35%), and the adipocyte markers *C/EBPα*, *Pparγ*, and *aP2* (40%), indicating an impairment of differentiation, an impairment in the maintenance of the fully differentiated adipocyte transcriptional program, or changes in cellular composition of the depot (Fig. 1*D*). Thus, whereas both IR and IGF1R are necessary for normal adipocyte gene expression, IR is more critical than IGF1R in maintenance of WAT mass, gene expression, and adipokine levels.

Differential Role of IR Versus IGF1R in BAT Development and Function

As in WAT, the IGF1R plays a modest role in BAT formation with a 25% reduction in BAT mass and normal histology in F-IGFRKO mice (Fig. 2*A* and *B*). By contrast, F-IRKO mice displayed a paradoxical 50% increase in BAT mass, with many cells containing unilocular lipid droplets, resembling white adipocytes (Fig. 2*A* and *B*). However, when both receptors were eliminated, there was a >85% reduction of BAT mass, and the remaining BAT was composed of a mixture of undifferentiated cells, small brown adipocytes, and some large unilocular fat cells (Fig. 2*B*).

Despite the white fat-like appearance of F-IRKO BAT, gene expression markers of white fat, such as *leptin* and *Hoxc8*, were not increased, nor was there a decrease in markers of brown fat, such as *Zic1* and *Lhx8*, or beige fat, such as *Tbx1* (Fig. 2*C*). Brown fat in F-IR/IGFRKO mice, in contrast, displayed decreases in *leptin* (60%) and *Hoxc8* (80%) and 4- to 33-fold increases in *Zic1*, *Lhx8*, and *Tbx1*. Expression of genes involved in BAT function, such as *Ucp1*, *Prdm16*, *Elovl3*, *Cidea*, *Dio2*, *Adrb3*, and *Tfam*, was reduced by 40–98% in F-IR/IGFRKO and F-IRKO BAT (Fig. 2*D*). Likewise, *Pparγ*, *Hsl*, *Glut4*, and *Fas* were decreased by 30–99% (Fig. 2*E*). In BAT lacking only the IGF1R, *Hsl*, *Fas*, and *Glut4* mRNAs were modestly reduced, but these did not reach statistical significance (Fig. 2*E*).

Consistent with the altered BAT mass, morphology, and gene expression, both F-IRKO and F-IR/IGFRKO mice were unable to maintain body temperature when placed at 6°C for 3 h; F-IRKO mice dropped their core body temperature by 5°C and F-IR/IGFRKO mice by >12°C (Fig. 2*F*). Although the lack of insulating subcutaneous adipose tissue or some change in shivering could contribute to the cold sensitivity of F-IRKO and F-IR/IGFRKO mice, expression of *Ucp1*, *Pgc1α*, *Elovl3*, *Cidea*, *Tfam*, and *Adrb3* were consistently lower in F-IRKO BAT compared with controls, even after cold exposure (Fig. 2*G*). Furthermore, F-IRKO BAT had decreased mitochondrial content and decreased oxygen consumption (Fig. 2*H*). F-IGFRKO mice, in contrast, were cold tolerant and had normal expression of thermogenic genes in BAT. These results indicate that although IGF1R is required for development of normal BAT mass, it is not essential for normal thermogenic function. The IR, in contrast, is dispensable for BAT development, but essential for the thermogenic function of BAT.

F-IRKO and F-IR/IGFRKO Mice Develop Diabetes That Is Reversed by Leptin Replacement

Both F-IRKO and F-IR/IGFRKO mice developed overt diabetes with random-fed blood glucose levels of ~500 mg/dL and 9- to 12-fold increases in insulin levels at 3 months of age (Fig. 3*A* and *B*). Likewise, F-IRKO and F-IR/IGFRKO mice were highly insulin resistant by insulin tolerance testing, even at doses of insulin of 2 units/kg (Fig. 3*C*). By contrast, F-IGFRKO mice had normal glucose and insulin levels, as well as normal insulin tolerance tests. F-IRKO and F-IR/IGFRKO mice also developed significant dyslipidemia with increased circulating TG and cholesterol levels, whereas FFA were increased in F-IR/IGFRKO mice only (Fig. 3*D*). Dyslipidemia was not observed in F-IGFRKO mice.

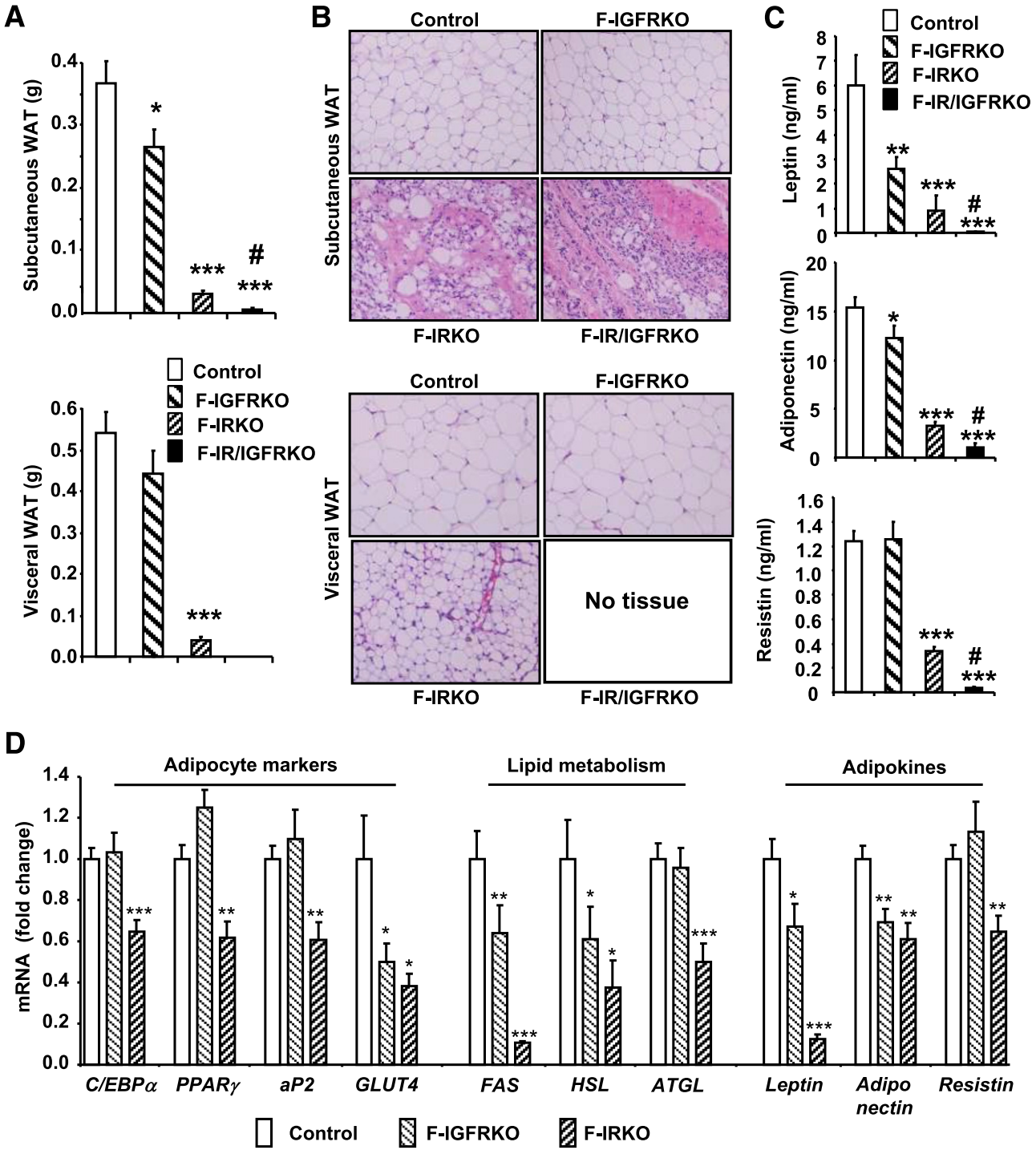

Figure 1—Lipodystrophy in mice lacking IR and IR/IGF1R in fat. *A*: Subcutaneous (inguinal) and visceral (epididymal) WAT weights in 3-month-old control, F-IGFRKO, F-IRKO, and F-IR/IGFRKO mice. Results are mean ± SEM of 12–30 animals per group. *B*: H&E-stained sections of subcutaneous and visceral adipose tissues from the same mice in *A*. *C*: Circulating leptin, adiponectin, and resistin levels in 3-month-old random-fed mice. Results are mean ± SEM of 7–17 animals per group. *D*: mRNA levels in visceral WAT from 3-month-old control, F-IGFRKO, and F-IRKO mice. Results are mean ± SEM of 6–10 animals per group. *Significant difference compared with controls (*$P < 0.05$, **$P < 0.01$, ***$P < 0.001$); #significant difference between F-IRKO and F-IR/IGFRKO mice, $P < 0.05$.

Leptin treatment has been shown to reverse hyperglycemia in mice and humans with lipoatrophic diabetes (18–21). In F-IRKO and F-IR/IGFRKO mice, leptin administration by subcutaneous infusion pumps results in a significant decrease in glucose levels within 4 days and almost complete normalization by 2 weeks (Fig. 3*E*). Leptin-treated mice also exhibited a 2- to 3-g weight loss during treatment, whereas saline-treated mice gained weight

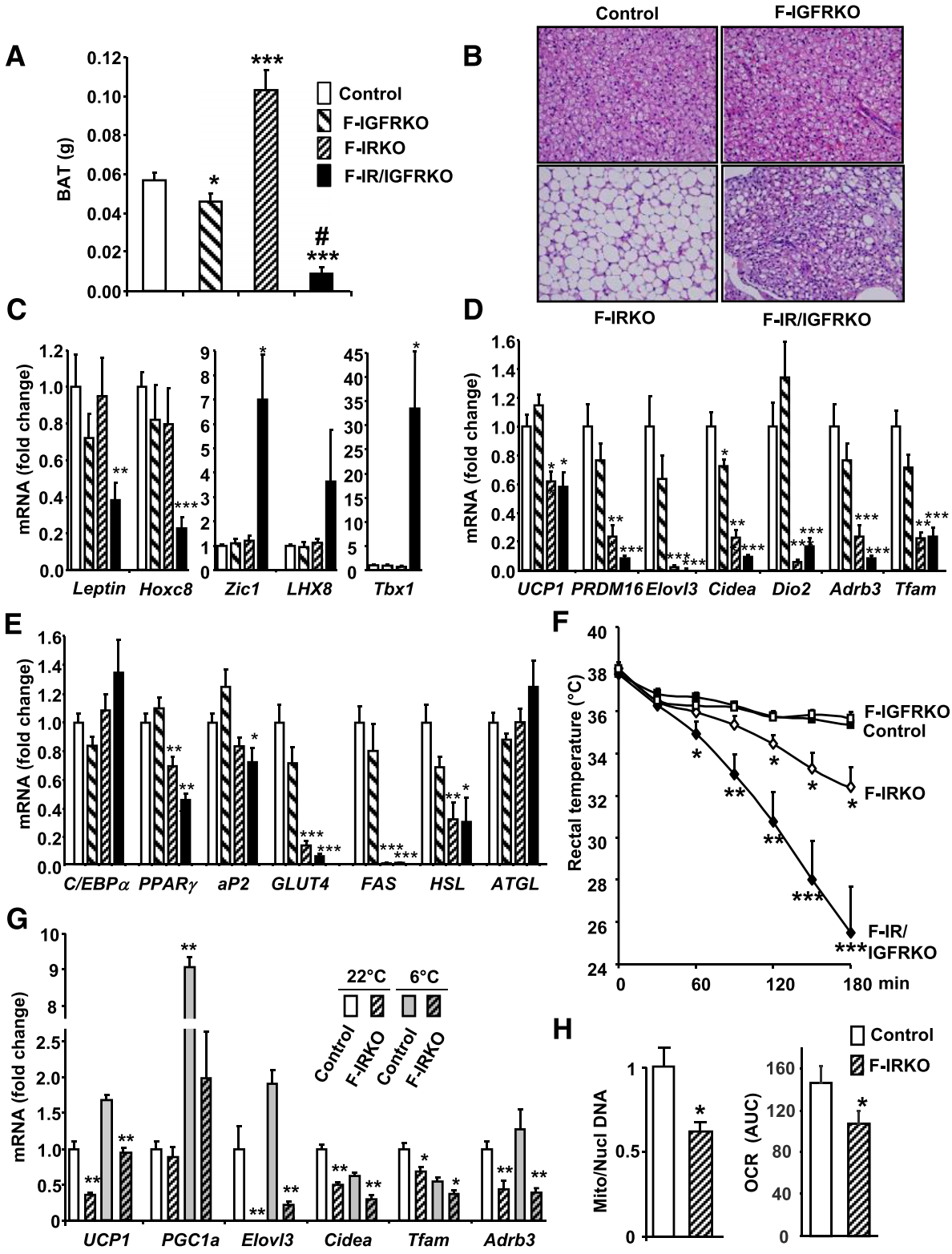

Figure 2— Importance of IR and IGF1R in BAT development and function. *A*: BAT weight in 3-month-old control, F-IGFRKO, F-IRKO, and F-IR/IGFRKO mice. Results are mean ± SEM of 12–30 animals per group. *B*: H&E-stained sections of BAT from the same mice in *A*. *C–E*: BAT mRNA levels from 3-month-old mice. Results are mean ± SEM of 6–10 animals per group. *F*: Rectal temperature measured in 3-month-old mice every 30 min for 3 h during exposure to a 6°C environment. Results are mean ± SEM of 10–15 mice per group. *G*: mRNA levels in BAT from 3-month-old mice at room temperature or exposed to a 6°C environment for 3 h prior to sacrifice. Results are mean ± SEM of five to six mice per group. *H*: Mitochondrial/nuclear DNA ratio (n = 9–11) and basal oxygen consumption rate (OCR; n = 4–6) in BAT from 3-month-old control and F-IRKO mice. Results are mean ± SEM. *Significant difference compared with controls (*P < 0.05, **P < 0.01, ***P < 0.001); #significant difference between F-IRKO and F-IR/IGFRKO mice, P < 0.05. AUC, area under the curve.

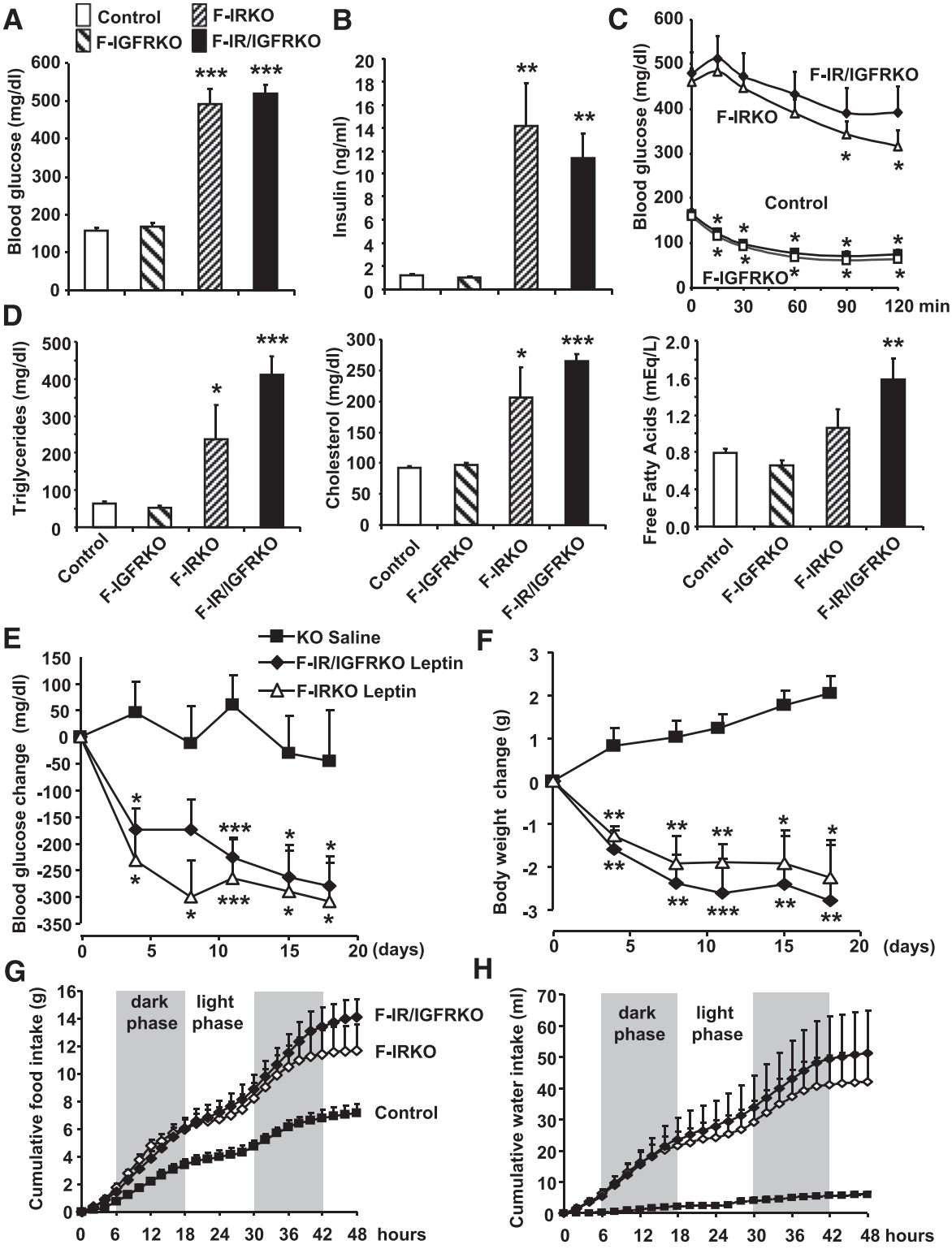

Figure 3—F-IRKO and F-IR/IGFRKO mice display lipoatrophic diabetes, which is reversible with leptin treatment. Blood glucose (*A*) and serum insulin levels (*B*) in random-fed 3-month-old control, F-IGFRKO, F-IRKO, and F-IR/IGFRKO mice. Results are mean ± SEM of 7–17 animals per group. *C*: Insulin tolerance test was performed in 3-month-old mice as described in RESEARCH DESIGN AND METHODS. Results are mean ± SEM of 12 animals per group. *D*: Serum TG, FFA, and cholesterol levels in random-fed mice at 3 months of age. Results are mean ± SEM of 7–17 animals per group. Blood glucose change (*E*) and body weight change (*F*) in random-fed 3-month-old F-IRKO and F-IR/IGFRKO mice during 2 weeks of leptin (10 μg/mouse/day) or saline treatment using Alzet osmotic minipumps. Saline-treated F-IRKO and F-IR/IGFRKO mice were pooled into a single control group. Results are mean ± SEM of six mice per group. Food intake (*G*) and water intake (*H*) were measured in metabolic cages in 3-month-old control, F-IRKO, and F-IR/IGFRKO mice. Results are mean ± SEM of 6–10 mice per group. $^{*}P < 0.05$; $^{**}P < 0.01$; $^{***}P < 0.001$.

(Fig. 3*F*), suggesting that reduced food intake may contribute to the decrease in blood glucose observed. Consistent with this, untreated F-IRKO and F-IR/IGFRKO mice were severely hyperphagic, with a food intake double that of controls (Fig. 3*G*) and concomitant polydipsia (Fig. 3*H*).

F-IRKO and F-IR/IGFRKO Mice Display β-Cell Hyperplasia

Elevated insulin levels were associated with massive pancreatic islet hyperplasia, which was easily detected by 3 months of age in F-IRKO and F-IR/IGFRKO mice (Fig. 4*A* and *B*). This correlated with increased β-cell proliferation as illustrated by the approximately fourfold increase in Ki67 labeling (Fig. 4*C* and *D*). No changes in insulin levels or pancreatic islet size were observed in F-IGFRKO mice. Expression of Angptl8/betatrophin (also known as RIFL or lipasin [22,23]) was increased by 1.8-fold in livers of 2.5-week-old lipodystrophic mice but returned to normal by 3 months of age. Expression of SerpinB1, a recently identified β-cell growth factor (24), was significantly increased by approximately twofold in livers from 3-month-old F-IRKO and F-IR/IGFRKO mice (Fig. 4*E*). Expression of SerpinB1 and Angptl8/betatrophin was not changed in WAT and BAT in 3-month-old mice (Supplementary Fig. 1).

F-IRKO and F-IR/IGFRKO Mice Display Ectopic Lipid Accumulation

To determine if the lipodystrophic phenotype of F-IRKO and F-IR/IGFRKO mice was associated with ectopic lipid accumulation, we measured TG levels in liver, muscle, and heart from control and knockout mice. Indeed, TG were elevated in both liver (25) and muscle and heart of lipodystrophic mice. TA muscle from 12-week-old F-IRKO and F-IR/IGFRKO mice showed ~2.5-fold increase in intracellular TG compared with control and F-IGFRKO muscles (Fig. 5*A*). Nile Red staining of muscle cross-sections confirmed this increase and indicated that the mitochondria-rich oxidative fibers specifically displayed the accumulation of lipid as evidenced by colocalization of Nile Red staining with the SDH-positive fibers (Fig. 5*B*). There was no difference in percent of oxidative fibers in the knockouts compared with controls (Fig. 5*C*). Expression of the glucose transporter Glut4 was decreased in F-IRKO and F-IR/IGFRKO muscle (Supplementary Fig. 2*A* and *B*), which could further exacerbate insulin resistance and glucose intolerance (26).

Interestingly, TA muscle weights were lower in F-IRKO and F-IR/IGFRKO mice (Fig. 5*D*), and muscle fiber size was significantly decreased compared with controls (Fig. 5*E*). Quantitation of the cross-sectional area showed that F-IRKO and F-IR/IGFRKO muscles had a higher percentage of small fibers ranging in size from 1,000 to 2,000 μm^2, compared with the normal distribution of muscle fiber size in control and F-IGFRKO mice (Fig. 5*F*). The muscle atrophy in these lipodystrophic mice was not explained by chronic upregulation of E3-ubiquitin ligases specific for muscle atrophy Atrogin-1 and MuRF-1, which were unchanged or decreased in F-IRKO and F-IR/IGFRKO mice (Supplementary Fig. 2*C*). Ectopic lipid accumulation in muscle is often associated with insulin resistance (27), but usually this occurs without muscle atrophy. We recently demonstrated that loss of IR in muscle causes significant muscle atrophy (15), and it is well known that hyperinsulinemia can induce IR degradation (28,29). In F-IRKO and F-IR/IGFRKO muscle, IR protein was decreased by ~90% compared with controls, and this occurred with no change in IR mRNA levels (Fig. 5*G–I*). In contrast to skeletal muscle, heart weight tended to be increased in 3-month-old lipodystrophic mice, although this did not reach significance. TG content of the hearts, however, was already elevated in F-IRKO and F-IR/IGFRKO mice, similar to the changes observed in skeletal muscle (Supplementary Fig. 3*A*). This occurred with no difference in blood pressure between control and F-IR/IGFRKO mice (Supplementary Fig. 4). At 52 weeks of age, heart size and weight of F-IRKO and F-IR/IGFRKO mice were significantly higher compared with the controls; however, heart TG content was not different among the groups, mirroring normalization of TG accumulation in the skeletal muscle at this age (Supplementary Fig. 3*B* and *C*). Taken together, these data demonstrate that the lipodystrophy in F-IRKO and F-IR/IGFRKO mice is associated with lipid accumulation in muscle and heart and muscle atrophy, probably secondary to downregulation of IR by the state of chronic hyperinsulinemia.

Hyperglycemia and Hyperlipidemia Develop Early but Improve With Age Despite Maintained Lipodystrophy

The natural history of the disease progression in F-IRKO and F-IR/IGFRKO mice is illustrated in Fig. 6 and documents sustained lipodystrophy throughout life. Subcutaneous/inguinal WAT, which appears first and was detectable in control mice even before weaning at 2.5 weeks of age, was already decreased by 50% in F-IR/IGFRKO mice at this time. From 5 to 52 weeks of age, subcutaneous WAT mass continually increased in controls, but remained decreased by >90% in F-IRKO mice and was hardly detectable in F-IR/IGFRKO mice at all ages (Fig. 6*A*). Likewise, visceral/perigonadal WAT, which was barely detectable at 2.5 weeks and gradually increased with age in controls, was reduced by >90% in F-IRKO mice and absent in F-IR/IGFRKO mice at all ages (Fig. 6*B*). Consistent with the low white fat mass, circulating leptin and resistin levels remained low even at 1 year of age (Supplementary Fig. 5).

In contrast to WAT, BAT undergoes significant development during embryogenesis and was present in similar amounts in 2.5-week-old control, F-IGFRKO, and F-IRKO mice, but was undetectable in F-IR/IGFRKO mice (Fig. 6*C* and Supplementary Fig. 6). In the latter, BAT weight remained <90% of control levels at 5 and 12 weeks of age and was undetectable in 1-year-old animals. As noted above, surprisingly, in 5-week-old F-IRKO mice, BAT was two times heavier than controls due to increased lipid accumulation, and BAT mass remained elevated up to 1 year of age in these mice. In F-IGFRKO mice, BAT mass was

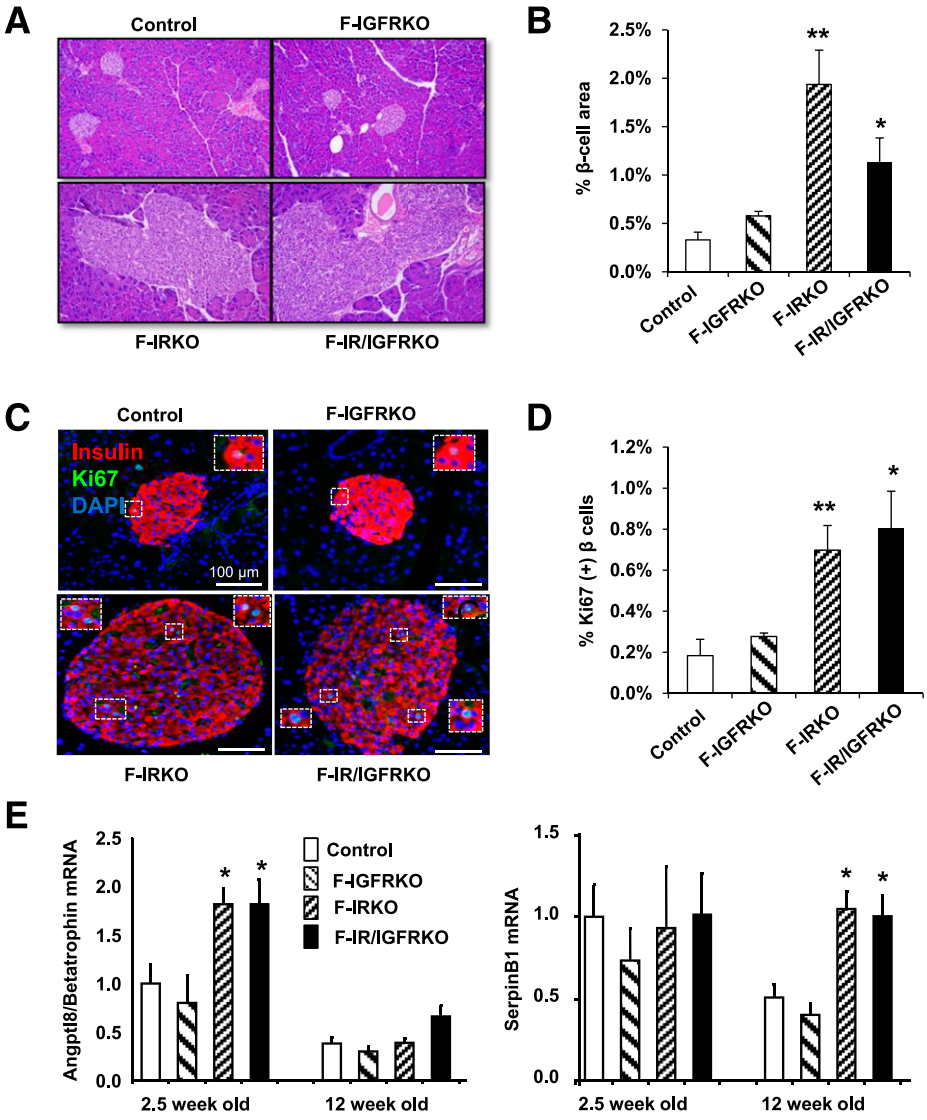

Figure 4— β-Cell hyperplasia in F-IRKO and F-IR/IGFRKO mice. *A*: H&E-stained pancreatic sections from control, F-IGFRKO, F-IRKO, and F-IR/IGFRKO mice at 3 months of age. *B*: Percent islet cell area as compared with total area of the pancreas. Results are mean ± SEM of four to five animals per group. *C*: Immunofluorescence staining for insulin, Ki67, and DAPI in pancreatic sections of 3-month-old mice. *D*: Percent of Ki67-positive β-cells. Results are mean ± SEM of four to five animals per group. *E*: Angptl8/betatrophin and SerpinB1 mRNA levels in livers from 2.5- and 12-week-old mice. Results are mean ± SEM of five to eight animals per group. *Significant difference compared with controls (*$P < 0.05$, **$P < 0.01$).

reduced by ~25% at 5 to 52 weeks of age, but was morphologically identical to controls (Fig. 6*C* and Supplementary Fig. 6).

Metabolic abnormalities were present in F-IRKO and F-IR/IGFRKO mice as early as they could be measured. Fed glucose levels were already significantly elevated in F-IRKO and F-IR/IGFRKO mice by 2.5 weeks of age (226 ± 34 and 231 ± 43 mg/dL vs. 145 ± 7 mg/dL in controls) and reached values of >500 mg/dL by 5 weeks of age. By 1 year of age, blood glucose levels unexpectedly improved (Fig. 6*D*). Circulating TG and FFA levels, which were elevated throughout the early months of life in F-IRKO and F-IR/IGFRKO mice, also returned toward normal by 1 year of age (Fig. 6*E* and *F*), whereas serum cholesterol levels remained elevated (Supplementary Fig. 7). The ectopic lipid deposition in skeletal muscle and heart and the decrease in muscle size observed in 3-month-old F-IRKO and F-IR/IGFRKO mice also normalized in 1-year-old mice, likely reflecting the changes in circulating lipid levels (Fig. 6*G* and Supplementary Figs. 3*B* and 8). However, by 1 year of age, both F-IRKO and F-IR/IGFRKO lipodystrophic mice developed cardiac hypertrophy with heart weights double that of control mice (Supplementary Fig. 4*B*).

Despite improved hyperglycemia, insulin levels, which were elevated by 10- to 15-fold as early as 2.5 weeks in F-IRKO and F-IR/IGFRKO mice, remained elevated throughout life (Fig. 6*H*). Likewise, at 1 year of age, F-IRKO and F-IR/IGFRKO mice remained hyperphagic, while their water

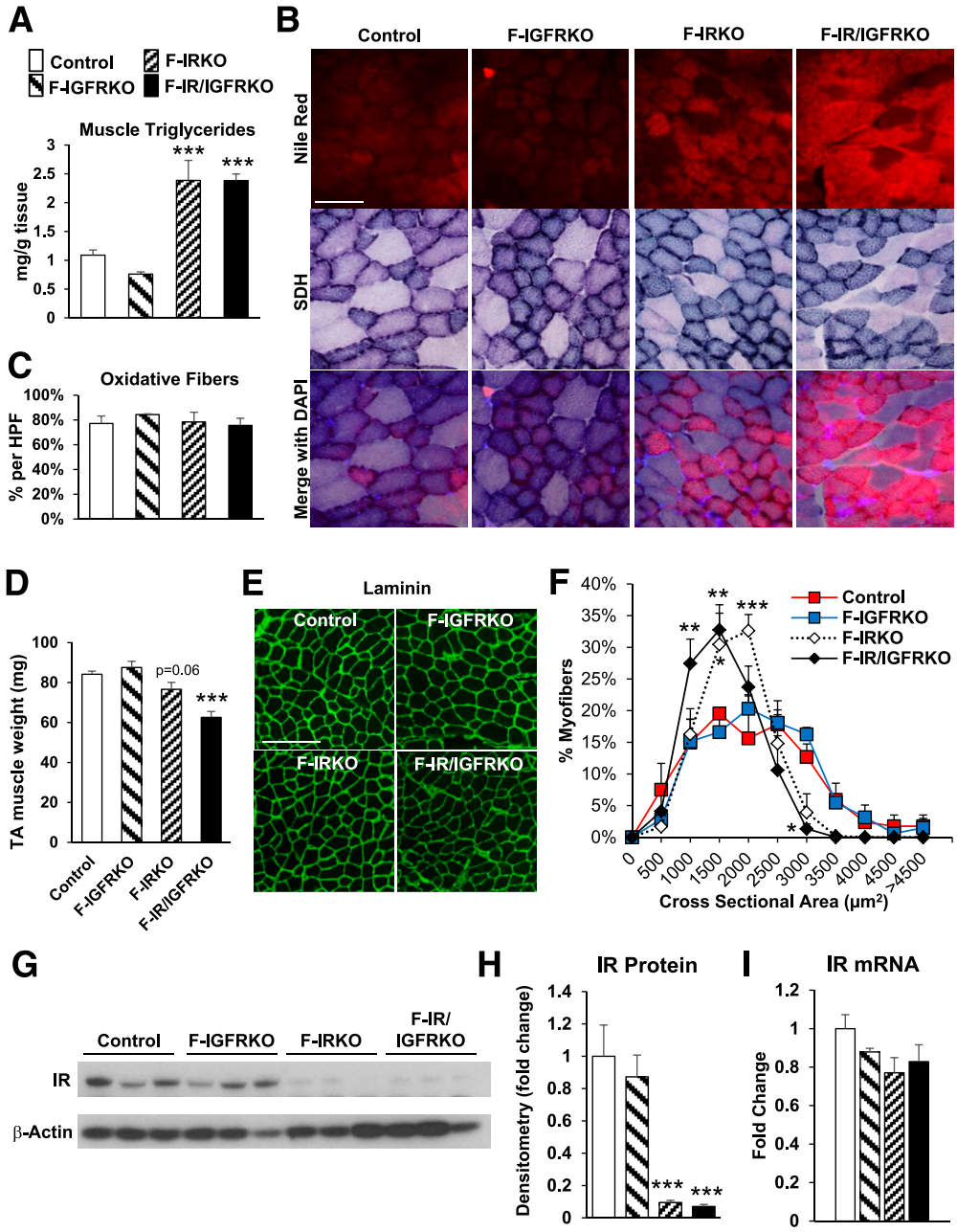

Figure 5—Ectopic lipid accumulation and decreased muscle size in F-IRKO and F-IR/IGFRKO mice. *A*: TG content in TA muscles from 3-month-old control, F-IGFRKO, F-IRKO, and F-IR/IGFRKO mice. *B*: Nile Red staining shows lipid accumulation colocalized with oxidative SDH-positive–stained (purple) myofibers in TA from F-IRKO and F-IR/IGFRKO (scale bar, 100 μm). *C*: Percent of SDH-positive oxidative (purple) fibers per high-power field (HPF). *D*: Weight of TA muscle from control and knockout mice at 3 months of age. Results are mean ± SEM of 12–30 animals per group. Laminin immunofluorescence (*E*) and cross-sectional area distribution (*F*) of laminin-stained fibers in TA muscles from 3-month-old control and knockout mice (scale bar, 200 μm). Results are mean ± SEM of three animals per group. Western blot (*G*) and densitometric quantification of protein levels (*H*) of IR in quadriceps muscle of 3-month-old mice. *I*: mRNA levels of IR in quadriceps muscle from control and knockout mice. Results are mean ± SEM of three to six animals per group. *Significant difference compared with controls (*$P < 0.05$, **$P < 0.01$, ***$P < 0.001$).

intake was dramatically reduced, reflecting improvement in blood glucose (Supplementary Fig. 9). β-Cell mass also continued to be highly increased in 1-year-old lipodystrophic mice, indicating persistence of insulin resistance (Fig. 6*I* and Supplementary Fig. 10). This massive islet hyperplasia occurred without increase in the expression of either putative β-cell growth factor, SerpinB1 and Angptl8/betatrophin, in liver at this age (Fig. 6*J*).

DISCUSSION

In the current study, we show that both insulin and IGF-1 signaling are essential for development and function of

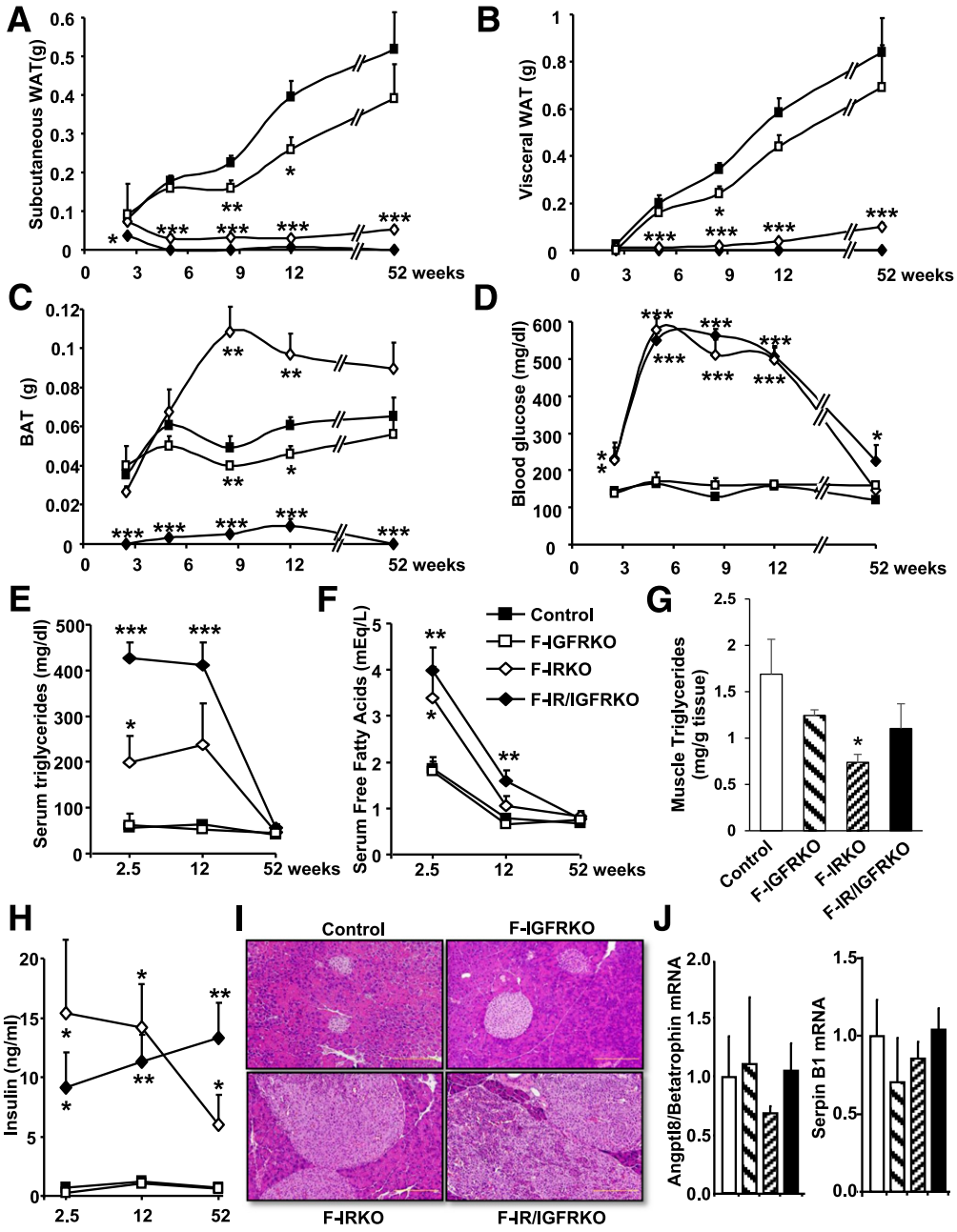

Figure 6—Disease progression in mice with IR and/or IGF1R knockout in fat. Subcutaneous (inguinal) WAT (*A*), visceral (epididymal) WAT (*B*), and interscapular BAT mass (*C*) from mice at 2.5, 12, and 52 weeks of age. Results are mean ± SEM of 7–17 animals per group. *D*: Blood glucose was measured in random-fed control, F-IGFRKO, F-IRKO, and F-IR/IGFRKO mice at the indicated ages from 2.5 weeks old to 1 year old. Results are mean ± SEM of 8–15 animals per group. Serum TG (*E*) and serum FFA (*F*) in random-fed mice at 2.5, 12, and 52 weeks of age. Results are mean ± SEM of 7–17 animals per group. *G*: TG content of TA muscles from 52-week-old control and knockout mice. Results are mean ± SEM of five to eight animals per group. *H*: Serum insulin levels were measured in random-fed control, F-IGFRKO, F-IRKO, and F-IR/IGFRKO mice at the indicated ages from 2.5 weeks old to 1 year old. Results are mean ± SEM of 8–15 animals per group. *I*: H&E-stained pancreatic sections from 1-year-old control, F-IGFRKO, F-IRKO, and F-IR/IGFRKO mice. *J*: Angptl8/betatrophin and SerpinB1 mRNA levels in livers from 52-week-old mice. Results are mean ± SEM of five to eight animals per group. **P* < 0.05; ***P* < 0.01; ****P* < 0.001.

adipose tissue, although these two receptors play different roles in white and brown fat. In WAT, IR is more dominant in both development and maintenance of normal mass and gene expression. The IGF1R also plays a role in gene expression in WAT, as well as in maintenance of normal serum leptin and adiponectin levels, but has little effect on tissue mass. Despite the modest role of the IGF1R alone, combined knockout of IR and IGF1R produces a more severe phenotype than knockout of IR alone, with greater reductions in fat mass and greater decreases in the

expression of adipocyte markers, adipokines, and lipogenic enzymes, indicating an interaction between these two complementary pathways. In BAT, in contrast, absence of IGF1R produces only a small decrease in mass and no decrease in function, as assessed by ability to maintain body temperature in the cold. By contrast, loss of IR alone produces an increase in BAT mass due to increased TG storage, but significant BAT dysfunction with inability to maintain body temperature in the cold. Again, IR/IGF1R double-knockout produces a profound decrease in BAT mass and profound cold intolerance, indicating a strong interaction between IR and IGF1R in BAT formation and function.

The striking difference and ultimate interaction between IR and IGF1R knockouts likely stems, at least in part, from differential expression of these two receptors during adipocyte development. The IGF1R is highly expressed in undifferentiated preadipocytes, whereas IR is low at this stage, and in mature adipocytes IR increases to high levels, dominating over IGF1R (3,5). Adiponectin expression is also the highest in mature adipocytes (30) and low in preadipocytes (31,32), leading to progressive gene recombination through the differentiation process. IGF1R may be deleted in the developing adipose tissues at a stage when expression of the IR with its overlapping pathways is high enough to rescue the absence of IGF1R, resulting in a minimal phenotype. Conversely, IR is probably deleted in differentiating adipocytes and in the presence of low IGF1R levels, producing a more severe phenotype. Lineage tracing studies using the adiponectin promoter indicate that adipocyte commitment in subcutaneous adipose tissue takes place during embryonic days 14–18, but in visceral adipose tissue occurs gradually during the postnatal period (33). The somewhat stronger phenotype in subcutaneous tissue may be due to the more sudden loss of insulin signaling in this depot, whereas a gradual decrease in visceral tissue may produce a milder phenotype.

We and others have shown that fat-specific knockout of genes using Cre-recombinase expressed under the aP2 promoter versus the adiponectin promoter can lead to different phenotypes. This is, in part, due to the higher expression and recombination efficiency of adiponectin-driven Cre and to the greater specificity of its expression in fat (10,11,13). In this study, it was impossible to directly measure recombination efficiency because the lipodystrophic mice have a profound loss of adipose tissue combined with infiltration by inflammatory cells and fibroblasts, resulting in a change in tissue composition that would obscure accurate gene recombination results.

Interestingly, deletion of IR and IGF1R using aP2-Cre versus Adipo-Cre produces different phenotypes. aP2-Cre F-IGFRKO mice have an increase in WAT mass and increased overall growth associated with a modest increase in circulating IGF-1 levels (8), whereas Adipo-Cre F-IGFRKO mice have modest reductions in both WAT and BAT mass but are of normal size, despite a 73% increase in circulating IGF-1 levels (Supplementary Fig. 11). Likewise, mice with knockout of the IR or both the IR and IGF1R created using the aP2-Cre have only a moderate reduction in WAT and exhibit improved glucose tolerance when challenged with a high-fat diet (6,9), whereas Adipo-Cre F-IRKO and F-IR/IGFRKO mice have almost no WAT and are overtly diabetic. This is similar to mice with *Pparγ* deleted using aP2-Cre, which display modest fat reduction and normal glucose levels (34,35), whereas mice with *Pparγ* deletion driven by Adipo-Cre exhibit almost a complete loss of WAT and BAT, marked hepatic steatosis, and severe diabetes (36).

The lipodystrophic syndrome observed in F-IRKO and F-IR/IGFRKO mice is similar to metabolic derangement of human generalized lipodystrophy including low leptin levels, marked insulin resistance, hyperlipidemia, and fatty liver disease (21,37). Leptin replacement reduces blood glucose levels and hepatic steatosis in human patients with lipodystrophy (38), and leptin replacement also normalizes blood glucose levels in F-IRKO and F-IR/IGFRKO mice. The effects of leptin are, at least in part, secondary to reduced food intake and can be mimicked by fasting alone (25).

The lipodystrophic phenotype present in the knockout mice is associated with insulin resistance and dramatically elevated insulin levels throughout life. This is due to massive β-cell hyperplasia, indeed the largest level observed in any of our tissue-specific knockout mice. Angptl8/betatrophin (22,23) and SerpinB1 (24) have recently been shown to be β-cell growth factors that contribute to the islet hyperplasia in insulin-resistant states. In our models of lipodystrophy, expression of Angptl8 and SerpinB1 in liver is modestly increased when the mice are young and may contribute to the increased β-cell proliferation. In contrast, at 1 year of age, F-IRKO and F-IR/IGFRKO mice continue to have massive β-cell hyperplasia despite normal expression levels of these putative β-cell growth factors, suggesting the possibility of other mechanisms driving β-cell growth in these lipodystrophic, insulin-resistant states.

Due to the inability to store fat in adipose tissues, lipodystrophic F-IRKO and F-IR/IGFRKO mice display ectopic lipid accumulation in liver and skeletal muscle. In muscle, this is associated with decreased fiber size and overall reduced skeletal muscle mass. This reduced muscle mass could reflect the increased muscle breakdown due to the uncontrolled diabetes in these mice or may be due to the marked downregulation of IR levels in skeletal muscle or some combination of these events (15). Muscle fiber size and intramyocellular TG normalized in older mice, as did many of the metabolic parameters including circulating glucose, fatty acid, and TG levels. In contrast, adipose tissue mass remained dramatically reduced and insulin levels remained elevated. The improvement in glucose levels is likely due to the worsening of fatty liver disease, which progressed to nonalcoholic steatohepatitis and development of dysplastic hepatic nodules with increased glycolysis and reduced gluconeogenesis. This is described in detail in the accompanying article by Softic et al. (25).

Whether this accounts for reversal of the other metabolic abnormalities remains to be determined.

In summary, insulin and IGF-1 signaling play critical and distinct roles in the development and function of white and brown fat. IR is most essential for formation and maintenance of WAT mass. IR is dispensable for development and/or maintenance of BAT mass, as long as IGF1R is present, but is essential for normal BAT-dependent thermogenesis. Lack of both IR and IGF1R in fat leads to severe generalized lipodystrophy of both WAT and BAT accompanied by diabetes, insulin resistance with increased β-cell mass, and ectopic lipid accumulation. The hyperglycemia and hyperlipidemia of this lipodystrophy disappear over time without recovery of lipodystrophy or reversal of insulin resistance. This model demonstrates the unique pathogenesis of the different features of the metabolic syndrome associated with lipodystrophy.

Funding. This work was supported by the Joslin Diabetes and Endocrinology Research Center Core Laboratories (P30-DK-036836); National Institute of Diabetes and Digestive Kidney Diseases (NIDDK) grants R01-DK-031036 and R01-DK-082659 to C.R.K., K12-HD-000850 to S.S., and R01-DK-67536 and R01-DK-103215 to R.N.K.; JDRF 3-APF-2014-182-A-N to A.E.O.; and NIDDK K08 Training Award K08-DK-100543 to B.T.O.

Duality of Interest. No potential conflicts of interest relevant to this article were reported.

Author Contributions. J.B. initiated the project, generated the data, and wrote the manuscript. S.S. generated the data and wrote the manuscript. A.E.O., M.T.K., A.K., R.N.K., and B.T.O. generated the data and reviewed the manuscript. C.R.K. oversaw the project, contributed to discussion, and helped write the manuscript. C.R.K. is the guarantor of this work and, as such, had full access to all the data in the study and takes responsibility for the integrity of the data and the accuracy of the data analysis.

References

1. Blüher S, Kratzsch J, Kiess W. Insulin-like growth factor I, growth hormone and insulin in white adipose tissue. Best Pract Res Clin Endocrinol Metab 2005; 19:577–587

2. Poulos SP, Hausman DB, Hausman GJ. The development and endocrine functions of adipose tissue. Mol Cell Endocrinol 2010;323:20–34

3. Boucher J, Tseng YH, Kahn CR. Insulin and insulin-like growth factor-1 receptors act as ligand-specific amplitude modulators of a common pathway regulating gene transcription. J Biol Chem 2010;285:17235–17245

4. Siddle K. Molecular basis of signaling specificity of insulin and IGF receptors: neglected corners and recent advances. Front Endocrinol (Lausanne) 2012; 3:34

5. Entingh-Pearsall A, Kahn CR. Differential roles of the insulin and insulin-like growth factor-I (IGF-I) receptors in response to insulin and IGF-I. J Biol Chem 2004;279:38016–38024

6. Blüher M, Michael MD, Peroni OD, et al. Adipose tissue selective insulin receptor knockout protects against obesity and obesity-related glucose intolerance. Dev Cell 2002;3:25–38

7. Guerra C, Navarro P, Valverde AM, et al. Brown adipose tissue-specific insulin receptor knockout shows diabetic phenotype without insulin resistance. J Clin Invest 2001;108:1205–1213

8. Klöting N, Koch L, Wunderlich T, et al. Autocrine IGF-1 action in adipocytes controls systemic IGF-1 concentrations and growth. Diabetes 2008;57:2074–2082

9. Boucher J, Mori MA, Lee KY, et al. Impaired thermogenesis and adipose tissue development in mice with fat-specific disruption of insulin and IGF-1 signalling. Nat Commun 2012;3:902

10. Lee KY, Russell SJ, Ussar S, et al. Lessons on conditional gene targeting in mouse adipose tissue. Diabetes 2013;62:864–874

11. Jeffery E, Berry R, Church CD, et al. Characterization of Cre recombinase models for the study of adipose tissue. Adipocyte 2014;3:206–211

12. Eguchi J, Wang X, Yu S, et al. Transcriptional control of adipose lipid handling by IRF4. Cell Metab 2011;13:249–259

13. Mullican SE, Tomaru T, Gaddis CA, Peed LC, Sundaram A, Lazar MA. A novel adipose-specific gene deletion model demonstrates potential pitfalls of existing methods. Mol Endocrinol 2013;27:127–134

14. El Ouaamari A, Kawamori D, Dirice E, et al. Liver-derived systemic factors drive β cell hyperplasia in insulin-resistant states. Cell Reports 2013;3:401–410

15. O'Neill BT, Lauritzen HP, Hirshman MF, Smyth G, Goodyear LJ, Kahn CR. Differential Role of Insulin/IGF-1 Receptor Signaling in Muscle Growth and Glucose Homeostasis. Cell Reports 2015;11:1220–1235

16. Debosch BJ, Chen Z, Saben JL, Finck BN, Moley KH. Glucose transporter 8 (GLUT8) mediates fructose-induced de novo lipogenesis and macrosteatosis. J Biol Chem 2014;289:10989–10998

17. Vernochet C, Damilano F, Mourier A, et al. Adipose tissue mitochondrial dysfunction triggers a lipodystrophic syndrome with insulin resistance, hepatosteatosis, and cardiovascular complications. FASEB J 2014;28:4408–4419

18. Shimomura I, Hammer RE, Ikemoto S, Brown MS, Goldstein JL. Leptin reverses insulin resistance and diabetes mellitus in mice with congenital lipodystrophy. Nature 1999;401:73–76

19. Ebihara K, Ogawa Y, Masuzaki H, et al. Transgenic overexpression of leptin rescues insulin resistance and diabetes in a mouse model of lipoatrophic diabetes. Diabetes 2001;50:1440–1448

20. Asilmaz E, Cohen P, Miyazaki M, et al. Site and mechanism of leptin action in a rodent form of congenital lipodystrophy. J Clin Invest 2004;113:414–424

21. Fiorenza CG, Chou SH, Mantzoros CS. Lipodystrophy: pathophysiology and advances in treatment. Nat Rev Endocrinol 2011;7:137–150

22. Yi P, Park JS, Melton DA. Betatrophin: a hormone that controls pancreatic β cell proliferation. Cell 2013;153:747–758

23. Gusarova V, Alexa CA, Na E, et al. ANGPTL8/betatrophin does not control pancreatic beta cell expansion. Cell 2014;159:691–696

24. El Ouaamari A, Dirice E, Gedeon N, et al. SerpinB1 Promotes Pancreatic β Cell Proliferation. Cell Metab 2016;23:194–205

25. Softic S, Boucher J, Solheim MH, et al. Lipodystrophy due to adipose tissue–specific insulin receptor knockout results in progressive NAFLD. Diabetes 2016; 65:2187–2200

26. Zisman A, Peroni OD, Abel ED, et al. Targeted disruption of the glucose transporter 4 selectively in muscle causes insulin resistance and glucose intolerance. Nat Med 2000;6:924–928

27. Pan DA, Lillioja S, Kriketos AD, et al. Skeletal muscle triglyceride levels are inversely related to insulin action. Diabetes 1997;46:983–988

28. Gavin JR 3rd, Roth J, Neville DM Jr, de Meyts P, Buell DN. Insulin-dependent regulation of insulin receptor concentrations: a direct demonstration in cell culture. Proc Natl Acad Sci USA 1974;71:84–88

29. Shanik MH, Xu Y, Skrha J, Dankner R, Zick Y, Roth J. Insulin resistance and hyperinsulinemia: is hyperinsulinemia the cart or the horse? Diabetes Care 2008; 31(Suppl. 2):S262–S268

30. Scherer PE, Williams S, Fogliano M, Baldini G, Lodish HF. A novel serum protein similar to C1q, produced exclusively in adipocytes. J Biol Chem 1995; 270:26746–26749

31. Hu E, Liang P, Spiegelman BM. AdipoQ is a novel adipose-specific gene dysregulated in obesity. J Biol Chem 1996;271:10697–10703

32. Körner A, Wabitsch M, Seidel B, et al. Adiponectin expression in humans is dependent on differentiation of adipocytes and down-regulated by humoral serum components of high molecular weight. Biochem Biophys Res Commun 2005;337: 540–550

33. Wang QA, Tao C, Gupta RK, Scherer PE. Tracking adipogenesis during white adipose tissue development, expansion and regeneration. Nat Med 2013;19: 1338–1344

34. He W, Barak Y, Hevener A, et al. Adipose-specific peroxisome proliferator-activated receptor gamma knockout causes insulin resistance in fat and liver but not in muscle. Proc Natl Acad Sci USA 2003;100:15712–15717

35. Jones JR, Barrick C, Kim KA, et al. Deletion of PPARgamma in adipose tissues of mice protects against high fat diet-induced obesity and insulin resistance. Proc Natl Acad Sci USA 2005;102:6207–6212

36. Wang F, Mullican SE, DiSpirito JR, Peed LC, Lazar MA. Lipoatrophy and severe metabolic disturbance in mice with fat-specific deletion of PPARγ. Proc Natl Acad Sci USA 2013;110:18656–18661

37. Huang-Doran I, Sleigh A, Rochford JJ, O'Rahilly S, Savage DB. Lipodystrophy: metabolic insights from a rare disorder. J Endocrinol 2010;207:245–255

38. Petersen KF, Oral EA, Dufour S, et al. Leptin reverses insulin resistance and hepatic steatosis in patients with severe lipodystrophy. J Clin Invest 2002;109: 1345–1350